RF-Over-Fiber Links With Very Low Noise Figure

Edward I. Ackerman, *Fellow, IEEE*, William K. Burns, *Fellow, IEEE*, Gary E. Betts, *Member, IEEE*,
Jianxiao X. Chen, *Member, IEEE*, Joelle L. Prince, Michael D. Regan, Harold V. Roussell, and
Charles H. Cox, III, *Fellow, IEEE*

(Invited Paper)

Abstract—Previously published analytical models for the noise figure of an amplifierless fiber-optic link fail to predict the measured performance, with a discrepancy of 1.1 dB at 1 GHz that increases to 2.3 dB by 12 GHz. We use an equivalent circuit to derive the effect of an additional source of noise not accounted for in earlier models: thermal noise arising from loss in the modulator's traveling-wave electrodes. The electrode thermal noise has a frequency dependence matching that of the link's noise figure, such that predictions using the improved model match the measured 1–12 GHz performance of a link with record low noise figure to within ∼0.4 dB across this band.

Index Terms—Analytical models, microwave photonics, noise figure, optical fiber links.

I. INTRODUCTION

ANTENNA remoting and other potential applications of analog fiber-optic links require both low noise figure (NF) and large dynamic range. Even a large link NF can be reduced using a very high-gain pre-amplifier; this can result, however, in reduced dynamic range. Consequently it is important to minimize the NF of an *amplifierless* link.

In a recent review paper [1] we summarized the state of the art in analog optical links and outlined the device technology advancements necessary to further improve their performance. Since the publishing of that paper, we developed new devices incorporating some of these recommended advances, and assembled from these a link with a record low broadband amplifierless NF of 3.4 dB at 2 GHz and < 7.5 dB across a broad bandwidth of 1–12 GHz [2].

In Section II of this paper, we show how the present state of the analog link modeling art fails to predict the measured NF data in [2]. Based on the frequency dependence of the discrepancy between the modeled and measured NF curves, we hypothesize an additional, heretofore ignored, source of thermal noise: ohmic loss in the long traveling-wave electrodes that enable efficient interaction between the light and the modulation signal. In Section III we derive expressions that summarize the effect of

this additional source of noise on the link's NF. Section IV analyzes the agreement between the measured performance of the record low-NF link in [2] and the NF predicted by the improved model. Awareness of the new noise term allows and requires us to state new conclusions (Section V) about what is necessary to achieve lower NF in future broadband amplifierless fiber-optic links.

II. REVIEW OF EXISTING MODEL WITH LOSSLESS ELECTRODES

Fig. 1 shows an equivalent circuit model for an external modulation link using a Mach–Zehnder modulator with *lossless* traveling-wave electrodes that have a characteristic impedance equal to the signal source impedance and that are terminated in this same impedance.

For the link in Fig. 1, previous papers provided expressions for the incremental small-signal gain [3]:

$$g_i \equiv \frac{i_d^2 R_S}{(v_s^2/4R_S)} = \left[\frac{\pi r_d T_{ff} P_I R_S}{2V_\pi(f)} |H_D(f)| \cos \phi \right]^2 \quad (1)$$

and the noise figure [1]:

$$\mathrm{NF} \equiv 10 \log \left[\frac{\overline{n_{\mathrm{out}}}}{kT_0 g_i} \right] = \frac{\overline{n_{\mathrm{out,th}}} + \overline{n_{\mathrm{out,RIN}}} + \overline{n_{\mathrm{out,shot}}}}{kT_0 g_i}. \quad (2)$$

All the terms in (1) are defined in the caption of Fig. 1 with the exception of $H_D(f)$, which represents the detector circuit's frequency response. In (2), k is Boltzmann's constant, T_0 is the standardized temperature of 290 K at which noise figure is defined [4], and $\overline{n_{\mathrm{out}}}$ is the link's total output noise power spectral density, which has components arising from thermal noise, the laser's relative intensity noise (RIN), and shot noise. Substituting g_i from (1) and expressions for all three noise spectral densities into (2) yields the full expression for noise figure given by equation 6 of [1]. The total output thermal noise power spectral density $\overline{n_{\mathrm{out,th}}}$ sets a lower limit to NF. In [1], which proceeded from the assumption that the modulator electrodes are *lossless*, this lower limit was expressed as

$$\mathrm{NF}_{\mathrm{min,lossless}} \equiv 10 \log \left[\frac{\overline{n_{\mathrm{out,th}}}}{kT_0 g_i} \right] = 10 \log \left[1 + x_1 + \frac{1}{g_i} \right] \quad (3)$$

where the unity term is dictated by the thermal noise from the signal source and the $1/g_i$ term arises from thermal noise generated in the detector circuit. The term x_1, which corresponds to an undefined term called simply "constant" in [1], arises from thermal noise generated in the electrode termination resistance.
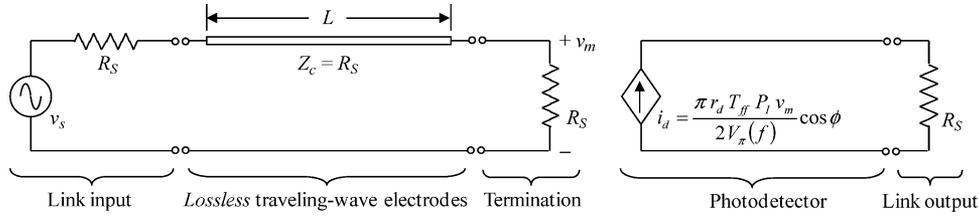
Fig. 1. Equivalent circuit model for an external modulation link using a Mach–Zehnder intensity modulator with *lossless* traveling-wave electrodes of characteristic impedance $Z_c = R_S$ and length L. v_s: signal source voltage; R_S: signal source and output load impedance; i_d: signal current amplitude at photodetector; r_d: photodetector responsivity; T_{ff}: insertion loss from input of modulator to photodetector; P_I: cw optical power at modulator input; $V_\pi(f)$: frequency-dependent modulator halfwave voltage; ϕ: modulator bias away from quadrature point.

This term is "constant" only in the sense that it does not depend on V_π, P_I, or any of the other parameters in (1) that directly affect g_i. This noise counter-propagates along the electrodes relative to the light, which it therefore modulates less efficiently than the signal source noise does. In the lossless-electrode case of Fig. 1, in which the electrode loss coefficient α is assumed to equal zero, quantification of this relative modulation inefficiency (e.g., see equation 19 in [5]) results in

$$x_{1,\text{lossless}} = \frac{\sin^2(\beta L)}{(\beta L)^2} \qquad (4)$$

where

$$\beta = \frac{2\pi f}{v_o} \qquad (5)$$

provided that the modulator electrodes of length L have been designed such that their guided-wave velocity at microwave frequency f matches that of light in the optical waveguides, which is v_o.

When the effect of loss in the modulator's traveling-wave electrodes is added to the model (i.e., when $\alpha \neq 0$), which is done in Section III, the term x_1 becomes somewhat more complicated and two additional terms x_2 and x_3 appear in the expression for $\text{NF}_{\min}$.

Returning to the case of a link with a lossless-electrode modulator, adding the well-established RIN and shot noise terms to (3) yields

$$\text{NF}_{\text{lossless}} = 10 \log \left[1 + \frac{\sin^2(\beta L)}{(\beta L)^2} + \frac{1}{g_i} \right.$$
$$\left. + \frac{[I_D^2 \text{RIN}(f) + 2q I_D] |H_D(f)|^2 R_S}{k T_0 g_i} \right] \qquad (6)$$

where I_D is the average value of the photodetector current and q is the electronic charge.

The link model with lossless electrodes that we have summarized in the above equations and elsewhere [1], [3], [6] has adequately predicted the measured noise figures of many links. In almost all of those cases, however, the noise figure was quite high, e.g., 12.5–15 dB across 1–9.5 GHz [7], indicating that laser RIN and/or shot noise were much more significant than any thermal noise term. One link modeled using (6) did have a measured noise figure low enough—4.2 dB at the frequency where the modulator and detector were resonantly impedance-matched to the link input and output, respectively [8]—to signify prominence of thermal noise terms. As shown by the dotted
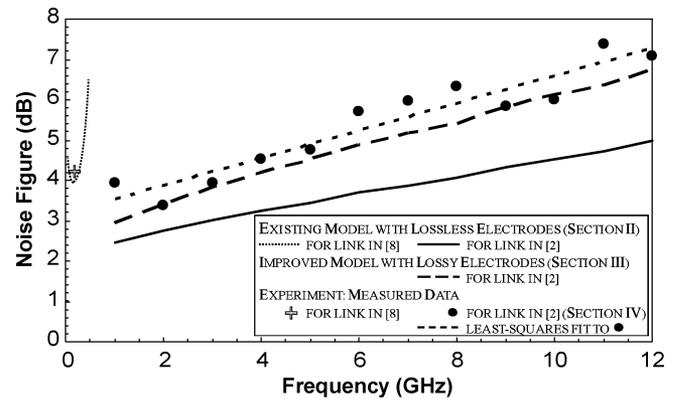
Fig. 2. Modeled versus measured noise figure results for links described in previous papers. The dotted and solid lines plot the noise figure predicted by the lossless model described in Section II for the links in [2] and [8], respectively. At frequencies >1 GHz, a least-squares fit to the measured data in [2] much more closely matches the predictions of the lossy model derived in Section III.

curve in the extreme left-hand portion of Fig. 2, (6) predicted a noise figure of ∼4.0 dB at 150 MHz for the link in [8]. From this agreement between the model and measurement we conclude that, not surprisingly, $\alpha L = 0$ must have been a reasonably accurate approximation of the actual loss in this modulator's electrodes at 150 MHz. (At such a low frequency, in fact, the traveling-wave effect disappears from any electrodes of reasonable length, causing $\beta \to 0$ and $\text{NF}_{\min} \to 3$ dB if $g_i \gg 1$ [6].)

Whereas (6) adequately predicts relatively high noise figures or low noise figures at sufficiently low frequencies, we have recently discovered its inadequacy at predicting low noise figures at microwave frequencies where αL cannot be approximated as zero. The solid curve in Fig. 2 shows the extent to which this lossless-electrode model underestimates the measured noise figure of a 1–12 GHz link that has been previously reported [2]. The higher of the two dashed curves in Fig. 2 is a least-squares fit to the measured noise figure data in [2]. At 1 GHz, the discrepancy between these two curves is its minimum: ∼1.1 dB. This discrepancy worsens with increasing frequency, and by 12 GHz the model underestimates the measured data's curve fit by 2.3 dB. The degradation of the lossless model's accuracy as frequency increases has led us to believe that the model ignores a source of noise whose magnitude increases with frequency. We have hypothesized that noise arising from ohmic loss in traveling-wave electrodes may have a frequency-dependent magnitude that accounts for the measured link noise figure. The lower
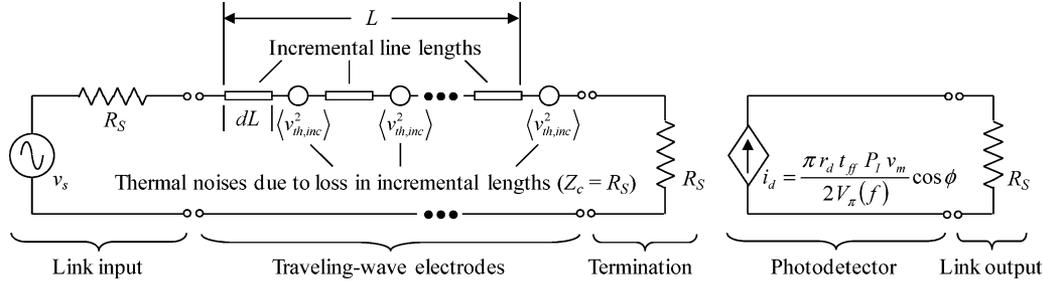
Fig. 3. Equivalent circuit model for an external modulation link that includes thermal noise arising from ohmic loss in the traveling-wave electrodes of a Mach–Zehnder intensity modulator. $\langle v_{\mathrm{th,inc}}^2 \rangle$: thermal noise spectral density arising from ohmic loss in the incremental length dL. Other parameters are as defined in the caption of Fig. 1.

of the two dashed curves in Fig. 2, which is a plot of an expression derived in Section III, appears to confirm this hypothesis.

III. IMPROVED ANALYTICAL MODEL OF LINK NOISE FIGURE

In this section, we derive an expression for link noise figure that includes the effect of ohmic loss in a Mach–Zehnder intensity modulator's traveling-wave electrodes, yielding the lower of the two dashed curves in Fig. 2.

A. Effect of Electrode Loss on Link Gain

The effect of the electrode loss on gain is reflected in (1) by the presence of the $V_\pi(f)$ term. The modulator's V_π has a frequency dependence dictated largely by the frequency dependence of loss in the electrodes (and, ultimately, on the extent to which the optical carrier and traveling-wave electrical signal velocities match one another [5]; the analysis here assumes perfect velocity matching), however, such that

$$V_\pi(f) = \frac{\alpha L}{1 - e^{-\alpha L}} \tag{7}$$

where the electrode loss coefficient α is itself a function of frequency [3], [5].

B. Effect of Electrode Loss on Thermal Noise From Termination Resistance

Including electrode loss in the model has two effects on noise figure. First, the expression for the effect of the thermal noise generated by the electrode termination resistance, which is represented by (4) for the lossless-electrode case, becomes more complicated [5]:

$$x_{1,\mathrm{lossy}} = \frac{(1 - e^{-\alpha L})^2 + 4\sin^2(\beta L)}{(\alpha L)^2 + 4(\beta L)^2}. \tag{8}$$

Second, two new constant terms x_2, x_3 arise from thermal noise generated by ohmic losses in the traveling-wave electrodes and dictate a minimum achievable noise figure exceeding what was previously postulated as the minimum in (3):

$$\mathrm{NF}_{\mathrm{min,lossy}} = 10 \log \left[1 + x_{1,\mathrm{lossy}} + x_2 + x_3 + \frac{1}{g_i} \right]$$
$$> \mathrm{NF}_{\mathrm{min,lossless}}. \tag{9}$$

The new terms x_2 and x_3 are derived in Sections III-C and III-D, respectively.

C. Modulation of Co-Propagating Light by Electrode Thermal Noise

We define the x_2 term in (9) as the portion of link noise figure due to modulation of light by *co-propagating* thermal noise that arises from loss in the modulator electrodes. We derive this term using the equivalent circuit in Fig. 3, in which the electrodes are modeled as a series of incremental pieces of transmission line each having length dL, characteristic impedance R_S, and ohmic loss that results in thermal noise spectral density $\langle v_{\mathrm{th,inc}}^2 \rangle$.

Anywhere one "cuts" the traveling-wave electrodes in the modulator of Fig. 3 yields an impedance of R_S looking into either of the two resulting sections of circuit. For instance, "cutting" the circuit between the end of the electrodes and the termination resistance R_S, the impedance looking towards the signal source from the termination end of the electrodes is also R_S. Therefore the spectral density of the noise imparted from the electrodes to the termination load must equal $4\,kT_0\,R_S$. Expressing this conclusion mathematically

$$4kT_0 R_S e^{-2\alpha L} + \frac{1}{L} \int_0^L \langle v_{\mathrm{th,inc}}^2 \rangle e^{-2\alpha(L-z)} dz = 4kT_0 R_S \tag{10}$$

where the first term on the left-hand side of (10) is the source's thermal noise density of $4\,kT_0\,R_S$, which is attenuated by $e^{-2\alpha L}$ in the total length of transmission line, and where the second term on the left-hand side is the sum of all the incremental thermal noise densities, each of which is attenuated by a quantity appropriate to the distance that noise voltage spectral density must propagate along the electrodes to reach the termination.

Note that the thermal noise arising from loss in one section of the electrodes has no effect upon or relation to the noise arising from loss in another section. Therefore, in (10) the contributions of the noise sources from the individual incremental lengths of lossy transmission line are tallied by summing the (scalar) squared magnitudes of the uncorrelated noise voltages. Tallying by first summing the voltages themselves and then squaring the scalar magnitude of that vector sum would be appropriate only if the individual noise sources were correlated.

Manipulation of (10) yields

$$\langle v_{\text{th,inc}}^2 \rangle = 8kT_0\alpha LR_S. \tag{11}$$

Each of these incremental thermal noise voltage spectral densities modulates the light as it *co-propagates* from its generation point along the electrodes *towards the termination*. (It also modulates the light as it *counter-propagates towards the signal source*; the effect of that modulation is derived in Section III-D below.) The efficiency with which each incremental noise voltage spectral density modulates the light depends on its generation point. For example, the leftmost incremental noise source in Fig. 3 modulates the light as efficiently as the signal does, i.e., with the same V_π, whereas the rightmost incremental noise source propagates towards the termination over an infinitesimal length of the electrodes and therefore "sees" a $V_\pi \sim \infty$. Specifically, two otherwise identical modulators with different electrode lengths will have the following relationship between their V_π's:

$$\frac{V_{\pi 1}}{V_{\pi 2}} = \frac{1 - e^{-\alpha L_2}}{1 - e^{-\alpha L_1}} \tag{12}$$

which approaches $L_2 \div L_1$ for small αL. Therefore, the effective V_π "seen" by an incremental noise source depends on its position relative to the co-propagating light according to

$$V_{\pi,\text{eff,co-prop}}(z) = V_\pi \frac{1 - e^{-\alpha L}}{1 - e^{-\alpha(L-z)}} \tag{13}$$

which approaches $V_\pi \cdot L \div (L - z)$ for small αL. The total output noise due to modulation of the light by *co-propagating* noise from the incremental noise sources is obtained by summing the resulting output noise power spectral densities:

$$\overline{n_{\text{out,electrodeloss,co-prop}}}$$
$$= \frac{1}{L} \int_0^L \left[\frac{\pi r_d t_{ff} P_I}{2V_{\pi,\text{eff,co-prop}}(z)} \right]^2 \frac{\langle v_{\text{th,inc}}^2 \rangle}{4} R_S dz$$
$$= 2kT_0 g_i \frac{\alpha}{(1 - e^{-\alpha L})^2} \int_0^L \left[1 - e^{-\alpha(L-z)} \right]^2 dz$$
$$= 2kT_0 g_i \frac{\alpha L - 2(1 - e^{-\alpha L}) + \frac{1}{2}(1 - e^{-2\alpha L})}{(1 - e^{-\alpha L})^2}. \tag{14}$$

As $\alpha L \to 0$, (14) reduces to the much simpler expression

$$\overline{n_{\text{out,electrodeloss,co-prop}}} \approx \frac{2}{3}\alpha L kT_0 g_i \tag{15}$$

and therefore

$$x_2 \approx \frac{2}{3}\alpha L. \tag{16}$$

D. Modulation of Counter-Propagating Light by Electrode Thermal Noise

How each of the incremental electrode thermal noise voltage spectral densities modulates the light as it *counter-propagates* from its generation point along the electrodes *towards the signal*

source is calculated similarly to (14). Again, the efficiency with which each incremental noise voltage spectral density modulates the light depends on its generation point. The effective V_π "seen" by an incremental noise source depends on its position relative to the counter-propagating light according to

$$V_{\pi,\text{eff,counter-prop}}(z) = V_\pi \frac{1 - e^{-\alpha L}}{1 - e^{-\alpha z}} \tag{17}$$

which approaches $V_\pi \cdot L \div z$ for small αL. Therefore, the total output noise due to modulation of the light by counter-propagating noise from the incremental electrode thermal noise sources is

$$\overline{n_{\text{out,electrodeloss,counter-prop}}}$$
$$= \frac{1}{L} \int_0^L \left\{ \left[\frac{\pi r_d t_{ff} P_I}{2V_{\pi,\text{eff,counter-prop}}(z)} \right]^2 \right.$$
$$\left. \times \frac{(1 - e^{-\alpha z})^2 + 4\sin^2(\beta z)}{(\alpha z)^2 + 4(\beta z)^2} \frac{\langle v_{\text{th,inc}}^2 \rangle}{4} R_S dz \right\}$$
$$= \frac{2kT_0 g_i \alpha}{(1 - e^{-\alpha L})^2}$$
$$\times \int_0^L (1 - e^{-\alpha z})^2 \frac{(1 - e^{-\alpha z})^2 + 4\sin^2(\beta z)}{(\alpha z)^2 + 4(\beta z)^2} dz. \tag{18}$$

In the most general case, the integral in (18) requires a numerical solution. At microwave frequencies of greatest interest, however, many modulators have sufficiently low αL such that

$$\overline{n_{\text{out,electrodeloss,counter-prop}}}$$
$$\approx \frac{2kT_0 g_i \alpha}{(1 - e^{-\alpha L})^2} \frac{4\alpha^2}{\alpha^2 + 4\beta^2} \int_0^L \sin^2(\beta z) dz$$
$$\approx \frac{4kT_0 g_i}{\alpha L} \frac{\alpha^2}{\alpha^2 + 4\beta^2} \left[1 - \frac{\sin(2\beta L)}{2\beta L} \right] \tag{19}$$

and therefore

$$x_3 \approx \frac{4}{\alpha L} \frac{\alpha^2}{\alpha^2 + 4\beta^2} \left[1 - \frac{\sin(2\beta L)}{2\beta L} \right]. \tag{20}$$

E. Summary of Model With Lossy Modulator Electrodes

Collecting the three "x" terms (8), (16), and (20), and adding the RIN and shot noise terms to (9) yields the most broadly general expression for the noise figure of an external modulation link using a Mach–Zehnder intensity modulator with traveling-wave electrodes:

$$\text{NF}_{\text{lossy}} \approx 10\log\left[1 + \frac{(1 - e^{-\alpha L})^2 + 4\sin^2(\beta L)}{(\alpha L)^2 + 4(\beta L)^2} + \frac{2}{3}\alpha L \right.$$
$$+ \frac{4}{\alpha L} \frac{\alpha^2}{\alpha^2 + 4\beta^2} \left(1 - \frac{\sin(2\beta L)}{2\beta L} \right) + \frac{1}{g_i}$$
$$\left. + \frac{(I_D^2 \text{RIN}(f) + 2qI_D)|H_D(f)|^2 R_S}{kT_0 g_i} \right] \tag{21}$$
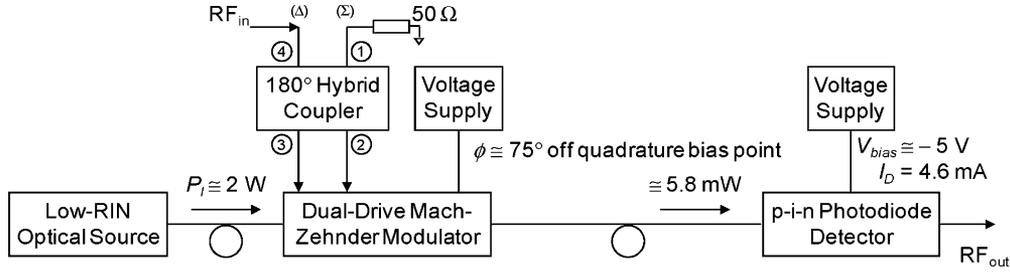
Fig. 4. Block diagram of a link [2] whose measured noise figure is used to validate the model updates presented in this paper.

where the link gain g_i is calculated using (1). It is important to note that in the lossless electrode case (i.e., where $\alpha = 0$), (21) reduces to the "lossless" expression (6).

IV. EXPERIMENT

Experimental confirmation of the heretofore unidentified terms in (21) requires a link in which the ordinarily dominant RIN and shot noise terms are greatly suppressed. An established method to minimize the impact of RIN and shot noise in an external modulation link and thereby achieve low NF is to "low-bias" the modulator [9]–[11]. As one moves the modulator's bias away from its quadrature point (where g_i is maximum) towards the minimum-transmission point on its transfer function curve, the RIN and shot noise contributions to the total output noise decrease faster than g_i decreases. Therefore, noise figure generally improves as one continually "lowers" the bias in this way. Before reaching the minimum-transmission bias point, however, the noise figure stops improving and begins to get worse because at some bias point the link gain has decreased to where the detector circuit thermal noise term, i.e., the $1/g_i$ term, has begun to dominate the link output noise. The higher the link gain is at the quadrature bias point, the lower one can bias the modulator before reaching this point where the $1/g_i$ term becomes significant, and the lower the resulting noise figure [11].

We used the noise figure results reported for a link in an earlier paper [2] to test the validity of the new terms derived in Section III. Fig. 4 shows a block diagram of the experimental link described in [2]. To ensure the highest possible gain at the quadrature bias point, and therefore the lowest possible noise figure when low biasing, the authors had taken the following steps in assembling this link:

i) obtained ~2 W from a master-oscillator power amplifier (MOPA) that had been engineered by Photonic Systems, Inc. for a low RIN of ~ −172 dB/Hz across 1–12 GHz;

ii) modulated this light using a lithium niobate Mach–Zehnder modulator also designed by Photonic Systems, Inc. for record low V_π across that same band: 0.93 V at 1 GHz and 1.4 V at 12 GHz;

iii) analytically determined and empirically confirmed that the noise figure would be minimized at a low bias point about 75° away from quadrature (where 90° off quadrature is the minimum-transmission bias).

Additional details about the laser, modulator, and detector used in this link appear elsewhere[1] [2]. Four details about the modulator, however, are important to note here. First, the modulator

had very long electrodes: $L = 14$ cm. This not only enabled the record low V_π but also made the device ideal for the purposes of this paper because it resulted in proportionately large electrode loss. Second, we judged the electrical–optical velocity mismatch to be ≤ 0.06, which degrades V_π by <10% at 12 GHz (the maximum frequency at which we planned to make measurements) and is therefore accounted for in the comparison of modeled to measured NF because measured V_π values were used in the modeling. Third, the modulator had "dual-drive" electrodes, requiring the use of a 180° hybrid coupler as shown in Fig. 4. And fourth, we define V_π for a dual-drive modulator as that which one would measure through an "ideal" hybrid coupler. In other words, V_π is the voltage that must be supplied at port 4 (see Fig. 4 for coupler port numbering) to move the optical output of the modulator from maximum to minimum transmission, assuming the coupler behaved "ideally"—i.e., with perfect amplitude balance and a 180° phase difference between ports 2 and 3 at all frequencies, and with no excess loss.

We define V_π of dual-drive modulators as described in the previous paragraph so that they can be evaluated independently of the hybrid couplers to which they are connected. We have previously defined an "ideality factor" to account for the effect of the coupler's characteristics on the gain and noise figure of a link that uses a dual-drive modulator [2]. Inserting this ideality factor appropriately into (4) yields the noise figure of a hypothetical amplifierless link using dual-drive traveling-wave electrodes that are *lossless*:

$$\mathrm{NF_{lossless}} = 10 \log \left[\frac{2}{|S_{34} - S_{24}|^2} \left(1 + \frac{\sin^2(\beta L)}{(\beta L)^2} \right) + \frac{1}{g_i} \right.$$
$$\left. + \frac{\left(I_D^2 \mathrm{RIN}(f) + 2q I_D \right) |H_D(f)|^2 R_S}{k T_0 g_i} \right]. \quad (22)$$

Similarly, inserting the ideality factor into (21) yields the noise figure of a link whose dual-drive modulator has *lossy* traveling-wave electrodes:

$$\mathrm{NF_{lossy}}$$
$$\approx 10 \log \left[\frac{2}{|S_{34} - S_{24}|^2} \left(1 + \frac{(1 - e^{-\alpha L})^2 + 4 \sin^2(\beta L)}{(\alpha L)^2 + 4(\beta L)^2} \right. \right.$$
$$+ \frac{2}{3} \alpha L + \frac{4}{\alpha L} \frac{\alpha^2}{\alpha^2 + 4\beta^2}$$
$$\left. \times \left[1 - \frac{\sin(2\beta L)}{2\beta L} \right] \right) + \frac{1}{g_i}$$
$$\left. + \frac{\left(I_D^2 \mathrm{RIN}(f) + 2q I_D \right) |H_D(f)|^2 R_S}{k T_0 g_i} \right] \quad (23)$$
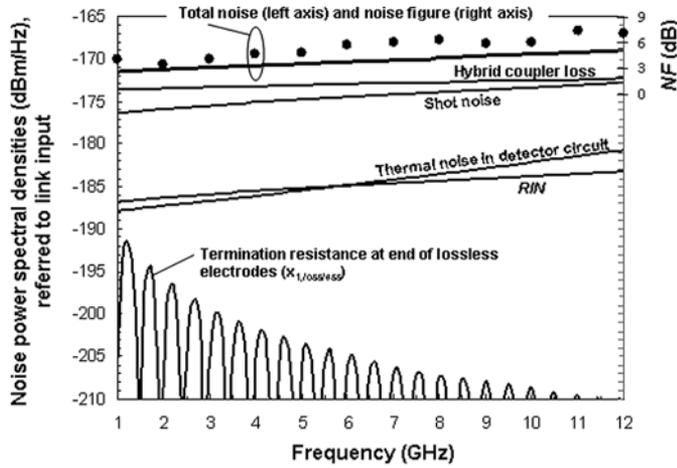
Fig. 5.   Modeled sources of noise in the link shown in Fig. 4, referred back to the link input, and measured link noise figure (NF). Key: ⎯⎯ noise power spectral densities that appear in the *lossless*-electrode modulator model (left axis); ⎯⎯⎯ total noise power spectral density predicted by the *lossless* model (left axis) and noise figure predicted by (22) (right axis), which is a repeat of the solid curve in Fig. 2; ● measured noise figure of link (right axis), also repeated from Fig. 2.

Fig. 6.   Modeled sources of noise in the link shown in Fig. 4, referred back to the link input, and measured link noise figure (NF). Key: ⎯⎯ noise power spectral densities in the *lossy*-electrode modulator model that are unchanged from the *lossless*-electrode model (left axis); ⎯ ⎯ ⎯ noise power spectral densities that appear only in the *lossy* model (left axis); ⎯⎯⎯ total noise power spectral density predicted by the lossy model (left axis) and noise figure predicted by (22) (right axis), which is a repeat of the dashed curve in Fig. 2; ● measured noise figure of link (right axis), also repeated from Fig. 2.

where in both (22) and (23) the link gain with the modulator biased ϕ degrees away from quadrature bias is

$$g_i = \left[\frac{\pi r_d t_{ff} P_I R_S}{2 V_\pi(f)} \frac{|S_{34} - S_{24}|^2}{2} \cos^2 \phi \right]. \qquad (24)$$

Note that for an "ideal" hybrid coupler, S_{34} and S_{24} would both have a magnitude of $1/\sqrt{2}$ and would have opposite sign, so that $|S_{34} - S_{24}|^2$ would equal 2, causing (22), (23), and (24) to reduce to (6), (21), and (1), respectively.

Figs. 5 and 6 both show the same measured noise figure data at 1, 2, ..., 12 GHz for the link in Fig. 4, as were reported in [2] and plotted with a greatly different vertical scale in Fig. 2. The other data plotted in the two figures are the power spectral densities of the various noise sources in the link, determined using the analytical model.

In the case of Fig. 5, we calculated all of the noise sources shown by the solid curves (the laser RIN, the shot noise arising from the photodetection process, and the thermal noise arising from loss in the hybrid coupler, the resistive termination of the modulator electrodes, and the detector circuit) using our model as it existed prior to the addition of the effect of loss in the modulator electrodes, i.e., using (22). The noise power spectral densities are all referred back to the link input by calculating their magnitude at the output of the link in dBm/Hz and subtracting $10 \cdot \log [g_i]$.

The uppermost curve in Fig. 5 is the total link output noise power spectral density, which is also referred back to the link input by subtracting $10 \cdot \log [g_i]$. According to (2), this total link output noise referred back to the link input is equal to NF + (−174 dBm/Hz). Therefore, by adding a right-hand axis with the same scale and with 0 dB noise figure corresponding to an output noise spectral density of −174 dBm/Hz, this one bold curve in Fig. 5 is made to represent both quantities, and is therefore the same as the solid curve in Fig. 2. The measured noise figure data points plotted in Fig. 5, which are also the same as

those in Fig. 2, likewise correspond to equivalent noise power spectral densities on the left-hand axis.

In Fig. 6, the unlabeled solid curves are unchanged relative to Fig. 5, but the additional effects of electrode loss, calculated using (15) and (20) and individually shown by the labeled dashed curves, are factored into the total shown by the bold dashed curve. Additionally, the "Termination resistance at end of lossy electrodes" curve, calculated using (8), replaces the corresponding curve in Fig. 5 ("Termination resistance at end of lossless electrodes"), which was calculated using (4).

Whereas Figs. 2 and 5 showed considerable discrepancy between the measured NF data and the lossless model, the analytical curves in Figs. 2 and 6 for NF including the effect of electrode loss agree substantially with the same measured data. The slope of the new model's curve appears to mirror the plot of least-squares fit to the measured data, with a nearly constant discrepancy of only ∼0.4 dB (see Fig. 2). What causes the improved model to underestimate the measured NF by this amount remains under investigation. Now that the discrepancies between modeled and measured NF are so small, it may be necessary to re-examine the validity of the general link NF expression derived previously in [1], [6], and [8]. Given the different statistical natures of the three types of noise in (2), for example, we may need to establish the extent to which it is completely versus only approximately valid to calculate the total noise by simply summing the spectral densities of the individual noise terms. Lastly, further understanding of the model's remaining shortcomings will be gleaned from comparing modeled and measured NFs of other ultra-low-NF links using low-V_π modulators with electrodes of other lengths as the demonstration of such links becomes more commonplace.

V. SUMMARY AND CONCLUSIONS

We have hypothesized that thermal noise generated by ohmic loss in the traveling-wave electrodes of an optical intensity mod-

ulator can significantly increase the lower limit to an ampli-fierless fiber-optic link's NF, and have updated our analytical model to account for this additional effect. We have further in-terpreted the substantial agreement shown in Figs. 2 and 6 be-tween the improved model and measured NF data as experi-mental confirmation of our hypothesis.

From this interpretation of the facts we conclude that we must amend our previous claims as to which photonic device devel-opments are necessary for lower amplifierless link NF. Whereas in [1] we stated simply that lower NF will require external in-tensity modulators with lower V_π, we did not specify in that paper how this should be accomplished. The link for which record low NF was reported in [2] was based on a modulator in which record low V_π had been achieved by maximizing the length over which the applied modulation signal acted upon light in the modulator's integrated optical waveguides. If the traveling-wave electrodes supporting this electro-optic interac-tion could have been somehow made to be *lossless*, the analyt-ical models published here and elsewhere predict $NF < 2.5$ dB at 1 GHz and <5.0 dB at 12 GHz (as shown by the solid curve in Fig. 2). Instead, the loss (αL) in those long electrodes dictated NF of at least 3.0–6.5 dB across this band. What is required for the lowest possible NF, therefore, is lower V_π in conjunc-tion with lower αL, implying either lower-loss electrodes (lower α) or greater efficiency of modulation over a given interaction length (i.e., a lower $V_\pi \cdot L$ product, such as is being explored in alternative materials such as electro-optic polymers).

ACKNOWLEDGMENT

REFERENCES

[1] C. Cox, E. Ackerman, G. Betts, and J. Prince, "Limits on the perfor-mance of RF-over-fiber links and their impact on device design," *IEEE Trans. Microw. Theory Tech.*, vol. 54, no. 2, pp. 906–920, Feb. 2006.
[2] H. Roussell, M. Regan, J. Prince, C. Cox, J. Chen, W. Burns, E. Ack-erman, and J. Campbell, "Gain, noise figure, and bandwidth-limited dy-namic range of a low-biased external modulation link," in *Proc. IEEE Int. Topical Meeting Microw. Photon.*, Victoria, Canada, Oct. 2007, pp. 84–87.
[3] E. Ackerman, G. Betts, W. Burns, J. Campbell, C. Cox, N. Duan, J. Prince, M. Regan, and H. Roussell, "Signal-to-noise performance of two analog photonic links using different noise reduction techniques," in *IEEE MTT-S Int. Microw. Symp. Dig.*, Honolulu, HI, Jun. 2007, pp. 51–54.
[4] H. Haus *et al.*, "IRE standards on methods of measuring noise in linear twoports," in *Proc. IRE*, Jan. 1959, vol. 48, pp. 60–68.
[5] G. Gopalakrishnan, W. Burns, R. McElhanon, C. Bulmer, and A. Greenblatt, "Performance and modeling of broadband LiNbO$_3$ trav-eling wave optical intensity modulators," *J. Lightw. Technol.*, vol. 12, pp. 1807–1819, Oct. 1994.
[6] C. Cox, *Analog Optical Links*.   Cambridge, U.K.: Cambridge Univ. Press, 2004.
[7] E. Ackerman, G. Betts, W. Burns, J. Prince, M. Regan, H. Roussell, and C. Cox, "Low noise figure, wide bandwidth analog optical link," in *Proc. IEEE Int. Topical Meeting Microw. Photon.*, Seoul, Korea, Oct. 2005, pp. 325–328.
[8] C. Cox, E. Ackerman, and G. Betts, "Relationship between gain and noise figure of an optical analog link," in *IEEE MTT-S Int. Microw. Symp. Dig.*, San Francisco, CA, Jun. 1996, pp. 1551–1554.
[9] G. Betts and F. O'Donnell, "Improvements in passive, low-noise-figure optical links," in *Proc. Photon. Syst. Antenna Applicat. Conf.*, Mon-terey, CA, 1993.
[10] M. Farwell, W. Chang, and D. Huber, "Increased linear dynamic range by low biasing the Mach-Zehnder modulator," *IEEE Photon. Technol. Lett.*, vol. 5, pp. 779–782, Jul. 1993.
[11] E. Ackerman, S. Wanuga, D. Kasemset, A. Daryoush, and N. Samant, "Maximum dynamic range operation of a microwave external modula-tion fiber-optic link," *IEEE Trans. Microw. Theory Tech.*, vol. 41, no. 8, pp. 1299–1306, Aug. 1993.

Edward I. Ackerman (M'87–SM'00–F'07) received the B.S. degree in elec-trical engineering from Lafayette College, Easton, PA, in 1987, and the M.S. and Ph.D. degrees in electrical engineering from Drexel University, Philadel-phia, PA, in 1989 and 1994, respectively.

From 1989 through 1994, he was employed as a Microwave Photonics En-gineer at Martin Marietta's Electronics Laboratory in Syracuse, NY, where he used low-loss narrowband impedance matching techniques to demonstrate the first amplifierless direct modulation analog optical link with RF gain ($+3.7$ dB at 900 MHz). From 1995 to July 1999, he was a Member of the Technical Staff at MIT Lincoln Laboratory, Massachusetts Institute of Technology, Cam-bridge, where he developed high-performance analog photonic links for mi-crowave communications and antenna remoting applications. During this time, he achieved the lowest noise figure ever demonstrated for an amplifierless analog optical link (2.5 dB at 130 MHz). While at Lincoln Laboratory, he also devel-oped and patented a novel linearization technique that uses a standard lithium niobate modulator with only one electrode to enable improved analog optical link dynamic range across broad bandwidths and at higher frequencies than other linearization techniques currently allow. Currently, he is Vice President of Research and Development for Photonic Systems, Inc., Billerica, MA. He has co-edited a book and has authored or co-authored three book chapters as well as more than 50 technical papers on the subject of analog photonic sub-system performance modeling and optimization. He holds two U.S. patents.

William K. Burns (M'80–SM'90–F'99) received the B.S. degree in engi-neering physics from Cornell University, Ithaca, NY, and the M.S. and Ph.D. degrees in applied physics from Harvard University, Cambridge, MA.

He is currently a Distinguished Staff Member at Photonic Systems, Inc., Bil-lerica, MA. From 1971 to 1999, he was a Research Physicist with the Naval Research Laboratory, Washington, DC, where he served as head of the Optical Waveguide Section of the Optical Techniques Branch. From 1999 to 2004, he was Chief Scientist at Codeon Corporation and its successor Covega. His re-search interests have primarily been in optical waveguides, lithium niobate in-tegrated optical devices—including the type of 2×3 optical coupler that PSI will design for this program—and the application of fiber-optic technology to signal processing, RF photonics, and sensors, in particular the fiber-optic gyro-scope. He has authored several book chapters in these areas and edited a book on fiber optic gyroscopes. He has contributed over 250 papers and presentations and been granted over 50 patents.

Dr. Burns has served on many conference committees, including Optical Fiber Communications, Integrated Photonics Research (conference chair in 1992), and IEEE LEOS. He was a topical editor for the *Journal of the Optical Society of America* from 1991 to 1994. He received NRL's Sigma Xi Award for Applied Science, and twice received NRL's Publication Award. In 1996, he was awarded the Institute of Navigation's Thurlow Award for contributions to the fiber optic gyroscope. He is a Fellow of the Optical Society of America.

Gary E. Betts (M'84) received the Ph.D. degree in electrical engineering/ap-plied physics from the University of California at San Diego in 1985.

He is currently a Senior Staff Engineer at Photonic Systems, Inc., Billerica, MA. His work involves component and system development in the field of analog optical links. Prior to joining Photonic Systems, he was a staff member at MIT Lincoln Laboratory, Massachusetts Institute of Technology, Cambridge, for 17 years. At MIT he worked primarily on lithium niobate integrated-optical modulators and analog fiber optic links. His work at MIT included design and fabrication of linearized modulators, high-frequency modulators, high-sensitivity modulators, and switch arrays; investigation of drift phenomena in lithium niobate; and research on semiconductor modulators and high powered semiconductor optical amplifiers. During the fiber optic boom and bust of 2000–2003, he co-founded a modulator company and served as its vice-president for a portion of its brief life. During his career he has authored or co-authored over 70 papers in integrated and fiber optics. He also holds five patents.

Jianxiao X. Chen (M'05) received the Ph.D. degree in electrical and computer engineering from the University of California at San Diego in 2006, where he investigated 10-GHz electroabsorption modulators, lithium niobate resonators, and an all-optical wavelength conversion based on four-wave mixing in a semiconductor optical amplifier.

He is currently a Principal Staff Engineer with Photonic Systems, Inc., Billerica, MA. While at Photonic Systems, he has been responsible for the technology transfer and implementation of a high-power, high-speed photodetector.

Joelle L. Prince (M'04) received the B.S. and M.Eng. degrees in applied and engineering physics from Cornell University, Ithaca, NY, in 1989 and 1991, respectively.

From 1992 through 1994, she was a Microwave Photonics Engineer at Martin Marietta's Electronics Laboratory in Syracuse, NY. From 1994 to 1996, she was with Micracor Inc., Acton, MA, where she developed the optically pumped microchip laser technology. From 1996 to 2000, she was with MIT Lincoln Laboratory, Massachusetts Institute of Technology, Cambridge, working on analog photonic links for microwave communications and antenna remoting applications and WDM optical communication networks. From 2000 to 2003, she was with AXSUN Technologies, Billerica, MA, where she developed optical spectral analysis equipment for WDM optical communication networks. Currently, she is a Principal Engineer at Photonic Systems, Inc., Billerica, MA. She holds one U.S. patent and has authored or co-authored over 15 papers on her research in the field of photonics.

Michael D. Regan received the B.S. degree in electrical engineering from Northeastern University, Boston, MA, in 2004.

He is currently an Electrical Project Engineer at Photonic Systems, Inc., Billerica, MA, where he has been implementing and testing optical and RF systems, including high gain/low noise figure optical links.

Harold V. Roussell received the Associate Engineering degree in electronic technology from Benjamin Franklin Institute of Technology in 1979 and the Bachelor of Science in electronic engineering technology from the University of Massachusetts Lowell in 1987.

He has been involved in developing many types of devices and systems using analog fiber optic transmission for nearly 30 years. From 1979 to 2000, he was employed at MIT Lincoln Labs as an Associate Technical Staff member. While at MIT Lincoln Labs, he worked on three major field deployed systems using fiber optics, one of which he took on the lead role for the fiber optical part in the system. His principal responsibilities included examining and testing different devices used in the field of analog fiber communications and reporting on the results at meetings. From 2000 to the present, he has worked for Photonic Systems, Inc., Billerica, MA, where he is currently Lead Microwave Photonic Engineer. His present responsibilities include researching and developing advanced measurement techniques used in fiber optical systems which have been instrumental in the setting of several analog link performance records. In addition, he has authored or co-authored over 20 technical papers and holds one patent.

Charles H. Cox III (M'78–SM'95–F'01) is President of Photonic Systems, Inc., Billerica, MA. He is one of the pioneers of the field that is now generally referred to as analog or RF photonics and has been active in the field for over 15 years. Among his notable technical achievements is the theoretical basis for and the first experimental demonstration of amplifierless optical links—using both direct and external modulation—with gain. Over this time he has participated in eight government–industry studies in the area of photonics, served on the committees of 16 conferences in a variety of roles including general chairman and technical program chair. He holds six U.S. patents, has given 45 invited talks on photonics, and has published over 70 papers. He is the author of the textbook *Analog Optical Links: Theory and Practice* (Cambridge University Press, 2004), has co-edited another book and has written two book chapters. He was elected a Fellow of the IEEE for his contributions to the analysis, design and implementation of analog links. He is also a member of Sigma Xi and the Optical Society of America.